



OPEN ACCESS

EDITED BY
Christopher David Taylor,
DNV GL, United States

REVIEWED BY
Mario Guagliano,
Politecnico di Milano, Italy
Da-Hai Xia,
Tianjin University, China

*CORRESPONDENCE
Erin K. Karasz,
ekarasz@sandia.gov

SPECIALTY SECTION
This article was submitted to Metal
Corrosion and Protection,
a section of the journal
Frontiers in Metals and Alloys

RECEIVED 16 August 2022
ACCEPTED 31 October 2022
PUBLISHED 17 November 2022

CITATION
Karasz EK, Montoya TD, Taylor JM,
Ross KA and Schaller RF (2022),
Accelerated corrosion testing of cold
spray coatings on 304L
in chloride environments.
Front. Met. Alloy 1:1021000.
doi: 10.3389/ftmal.2022.1021000

COPYRIGHT
© 2022 Karasz, Montoya, Taylor, Ross
and Schaller. This is an open-access
article distributed under the terms of the
[Creative Commons Attribution License
\(CC BY\)](https://creativecommons.org/licenses/by/4.0/). The use, distribution or
reproduction in other forums is
permitted, provided the original
author(s) and the copyright owner(s) are
credited and that the original
publication in this journal is cited, in
accordance with accepted academic
practice. No use, distribution or
reproduction is permitted which does
not comply with these terms.

Accelerated corrosion testing of cold spray coatings on 304L in chloride environments

Erin K. Karasz^{1*}, Timothy D. Montoya¹, Jason M. Taylor¹,
Kenneth A. Ross² and Rebecca F. Schaller¹

¹Sandia National Laboratories, Albuquerque, NM, United States, ²Pacific Northwest National Laboratory, Richland, WA, United States

Cold spray is an advanced metal manufacturing technique applied across many fields for a wide range of functions. Low heat input and compressive stresses induced into the substrate by the cold spray process makes it a promising choice for protective corrosion resistant coatings. One potential application for cold spray is as a protective coating against corrosion for spent nuclear fuel (SNF) interim dry storage canisters. As these canisters are currently stored at interim storage locations longer than originally intended, chloride induced stress corrosion cracking has been identified as a high priority knowledge gap, specifically with respect to prolonging or extending canister lifetimes (Teague et al., 2019). The high deployability of cold spray, for which nozzles have been developed for application in constrained spaces, in conjunction with beneficial properties inherent to cold spray makes this a good candidate for a corrosion protection coating on SNF canisters. This work explores a pathway to rapidly down-select cold spray coatings for canisters by focusing on the corrosion properties. Specifically, this study examines the corrosion protection abilities of nickel and nickel-based alloy cold spray coatings on 304 L stainless steel in chloride rich environments through electrochemical scans and ferric chloride pitting tests (ASTM G48 Method A). It was shown that the porosity of the coating, the processing gas, material selection, and deformation in the substrate all impact the corrosion behavior of cold spray coatings and are areas where optimization could reduce potential materials degradation, enabling enhanced coatings development.

KEYWORDS

corrosion, cold spray, stainless steel, nickel, chloride

Introduction

Cold spray is an advanced manufacturing technique, operating at lower temperatures than other additive manufacturing (AM) and thermal spray techniques, that adheres powder metal (or composite) particles to a substrate, and each other, *via* plastic deformation (Smith et al., 2016; Champagne et al., 2018; Yin et al., 2018). This is distinct from other advanced manufacturing techniques that melt the particles during processing. The lower heat input can prevent temperature-dependent crystalline

TABLE 1 Compositions of cold spray powders as compared to the substrate in weight percent.

	Inconel 625–2	Super C	Nickel	304 L substrate
C	0.02%	0.02%	≤0.01%	0.003%
Co	0.09%	0.2%	—	—
Cr	21.47%	23.2%	—	18.19%
Cu	—	—	—	0.36%
N	—	—	—	0.07%
Ni	Balance	Balance	>99.9%	8.05%
Mo	9.06%	17.7%	—	0.27%
Mn	0.04%	0.7%	—	1.30%
P	0.0%	0.002%	—	0.028%
S	0.0%	0.004%	≤0.001	0.001%
Si	0.07%	0.5%	—	0.34%
Fe	4.62%	0.6%	≤0.14%	Balance
Al	0.04%	—	—	—
B	0.001%	0.003%	—	—
Nb	3.65%	—	—	—
O	0.024%	—	≤0.4%	—
V	—	0.30%	—	—
W	—	0.26%	—	—

transformations, (Champagne and Helfrich, 2014a) and help prevent oxidation and vaporization (Papyrin, 2001). Cold spray can induce compressive residual stresses in the substrate (Luzin et al., 2020), thought to be beneficial for resistance to corrosion and subsequent stress corrosion cracking (SCC) (Toribio, 1998). The ability to use multiple types of powder at once as well as blend powders opens possibilities to functionally grade coatings and introduce filler or hardening particles (Sova et al., 2013). It also has the ability to be deployed to the field (Nardi, 2019). Applications for cold spray include medical devices (Lee et al., 2013; Al-Mangour et al., 2014; Vilardell et al., 2015; Dosta et al., 2018), aircraft (Champagne, 2008; Leyman and Champagne, 2009; Soboń, 2018; Yin et al., 2018), automobiles (Soboń, 2018; Yin et al., 2018), and nuclear power (Sohag et al., 2017; Ševeček et al., 2018; Umretiya et al., 2020; Yeom et al., 2020;

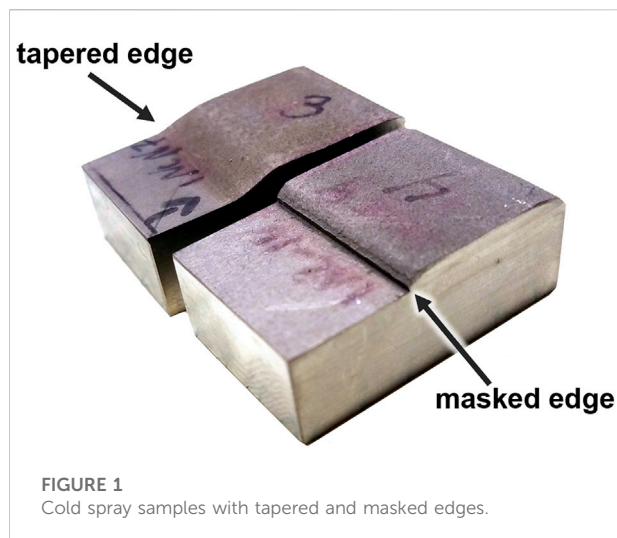
Yeom and Sridharan, 2021). In some cases, cold spray has been explored as a technique for fabricating light weight components (Singh et al., 2021), for structural repairs (Champagne and Helfrich, 2014b; Widener et al., 2018), and in others as a coating for temperature protection (Karthikeyan, 2005; Singh et al., 2012), and a barrier between the substrate and environment for erosion and corrosion prevention and repair (Bala et al., 2013; Hassani-Gangaraj et al., 2015; Widener et al., 2015; Jiang et al., 2020; Kumar et al., 2020). Currently, there is a lack in studies within the literature on the corrosion behavior of these coatings.

This work was focused on cold spray as a corrosion prevention or mitigation technique for spent nuclear fuel (SNF) canisters. SNF is often placed in canisters made from 304 or 316 stainless steel for dry storage. In interim storage, the canisters are placed in overpacks where ambient air circulates through vents in the overpack to passively cool the canisters. These canisters are located at interim storage facilities across the U.S., with many located in near-marine environments. As these canisters cool, chloride salts are deposited with dust onto the canister surface from the circulating air and, over time, the surface temperature of the canister will reach a temperature where the surface relative humidity (RH) can become greater than the deliquescent RH. This will cause the salts to deliquesce and form liquid brines, increasing the risk for corrosion. The presence of corrosion on these stainless steel canisters poses the possibility of stress corrosion cracking, acting as likely sites for crack initiation. As such, there exists a need to develop potential corrosion mitigation and repair strategies for SNF canister. The use of cold spray as a corrosion mitigation and repair technique for SNF canisters is attractive both for its deployability and the compressive stresses it induces. This technique may feasibly extend the canister lifetime, thus aiding in the expansion of the carbon-free nuclear power industry.

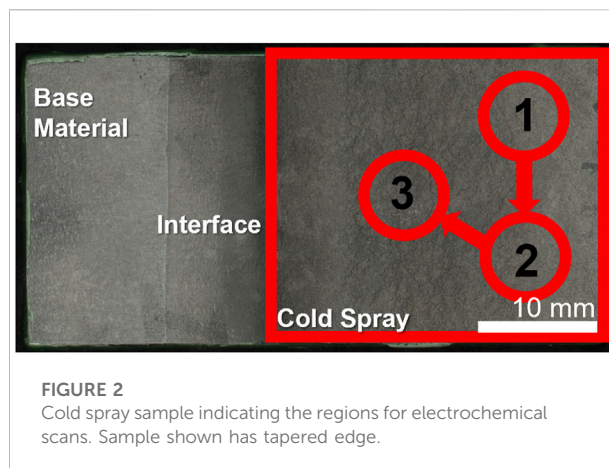
However, there are several known properties of cold spray that may need further consideration prior to implementation as a coating, particularly as a corrosion barrier such as in the case of SNF canisters. Galvanic coupling effects between the selected cold spray material and the substrate should not be ignored, nor the galvanic coupling between any filler particles and the primary coating constituents although this has largely not been explored

TABLE 2 Process parameters and equipment used for cold spray coatings.

Cold spray material	Process gas	Cold spray system	Gas pressure (MPa)	Gas temperature (°C)	Powder feed setting (RPM)	Average per layer thickness (mm)
CP Nickel	Nitrogen	Plasma Giken	4	900	1	0.178
CP Nickel	Helium	CGT 4000	3	445	1	0.178
Inconel 625	Nitrogen	Plasma Giken	4	950	1.25	0.152
Inconel 625	Helium	Plasma Giken	3	850	1.25	0.165
Super C	Nitrogen	Plasma Giken	4	950	1.25	0.114
Super C	Helium	Plasma Giken	3	850	1	0.076



in literature and not for nickel or nickel-based alloys on stainless steel. Porosity in AM metals is known to aid corrosion initiation (Bala et al., 2013; Hassani-Gangaraj et al., 2015; Schaller et al., 2017) and cold spray is known to have porosity, which can fluctuate with material selection and processing parameters (Bala et al., 2013; Hassani-Gangaraj et al., 2015; Champagne et al., 2018). This may lead to exacerbated corrosion combined with the galvanic coupling. If the porosity is interconnected, it could render a coating ineffectual. The intersplat region (i.e., the region between deformed particles) is specifically of concern as it has been shown to be more susceptible to corrosion and is connected to pores (Qu et al., 2022). Moreover, a continuous pathway from the exposed surface, through the cold spray and to the substrate, could form along intersplat boundaries, analogous to intergranular corrosion. The kinetic energy involved with the particle impact can create a nanocrystalline structure on the edges of the particles (Rokni et al., 2017). This impact also has the possibility to influence the underlying substrate microstructure, creating regions of high deformation, twinning, or microstructural phase changes, i.e., strain-induced martensite in an austenitic substrate (Yeom et al., 2020). These changes could negatively impact the local corrosion resistance, in the case of austenitic stainless steel, strain-induced martensite would be more susceptible than the neighboring austenite matrix. Similar to other AM processes, residual stress is a concern (Sample et al., 2020). For AM processes like laser-based powder bed fusion, residual stress inherent from the process has been shown sufficient to induce SCC in aggressive corrosion conditions (Karasz et al., 2021). Even though cold spray induces compressive residual stress in the substrate directly beneath, it is unknown how compensation of this induced stress at coating edges may affect the distribution of residual stress and subsequent corrosion.



This work applies accelerated testing in aggressive conditions to begin developing a process for evaluating cold spray coatings as a corrosion prevention mechanism for 304 L stainless steel. The goal of this work is to help enable the optimization of cold spray specific parameters such as carrier gas, material, and edge type. Coating materials were chosen for historically pairing well with 304 stainless steel as it relates to galvanic coupling (ToolBox, 2009). Additionally, materials were chosen for their large body of research as a cold spray material and their spray parameters having already largely been optimized as a coating on stainless steel (Jiang et al., 2020).

Accelerated standardized testing for sweater environments were selected to explore and characterize corrosion properties of cold spray patches. Electrochemical potentiodynamic scans in 0.6 M sodium chloride solution are performed to evaluate the cold spray and substrate materials. Full immersion testing in ferric chloride, following ASTM G48 Method A, is also employed to evaluate the pitting susceptibility of the exposed interface between the base and cold spray materials which is often neglected in the existing research. Pre exposure metallography was carried out to evaluate porosity and surface roughness. Post exposure characterization was conducted to examine microstructure and hardness. The correlations to corrosion behavior under accelerated tests were subsequently explored. Implications for optimization of cold spray patches are discussed.

Materials and methods

Materials

Wrought 304 L was used as a substrate material. The powders deposited were either Inconel 625–2, Super C, or commercially pure nickel. The alloys are generally considered to have good corrosion resistance (Huang et al., 2007). Nickel

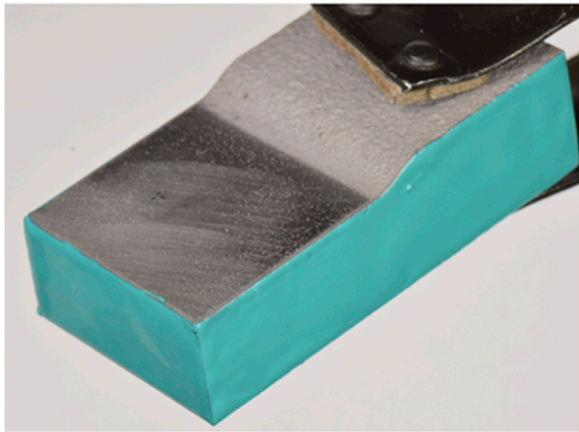


FIGURE 3
Cold spray sample with tapered interface, coated on sides with epoxy, being held by clamp.

serves as a comparative for corrosion purposes but is also much softer and easier to cold spray compared to the alloys. These materials have also historically been considered a low galvanic corrosion risk when paired with stainless steel (ToolBox, 2009). The compositions of the cold spray powders used are given in Table 1. Nickel, being the softest powder material in this study, is expected to deform easier and thus result in less porosity compared to the Inconel and Super C. The increased molybdenum content in Super C compared to the Inconel provides higher work hardenability and resistance to deformation (Eiselstein and Tillack, 1991; Huang et al., 2007).

Cold spray coatings presented in this work were fabricated using parameters and equipment described in Table 2. Cold spray

parameters were chosen based on previous optimizations (Jiang et al., 2020; Ross et al., 2021). Both nitrogen and helium carrier gasses were employed for comparison. Helium carrier gas may enable increased particle velocity due to the higher critical velocity of helium compared to nitrogen. This could result in increased plastic deformation and reduced porosity and surface roughness.

Two patch edge types were examined: tapered and masked. As seen in Figure 1 the tapered edge, the cold spray layer tapers down from the full thickness of the cold spray to the base material while the masked edge drops off sharply. Samples of both interface type, tapered and masked, were tested for all material and gas combinations with the exception of Inconel-helium and Super C-nitrogen which only tapered interface samples were available.

The coating surface roughness was measured using a Keyence VR-5200. The porosity was evaluated using ASTM E2109-01 (ASTM, 2021). Cross sections of the samples were polished, and three images were collected with the Keyence VR-5200. The images were processed with ImageJ to calculate the porosity (Schneider et al., 2012).

Electrochemical testing

Samples were tested in the as-sprayed and ground conditions. The substrate material was also tested for comparison purposes. Ground samples were ground with silicon carbide paper to 1,200 grit finish, rinsed with deionized water and dried with nitrogen. An o-ring was fixed to the sample surface using DevCon 5-min epoxy leaving a test area ranging from 0.1 to 0.3 cm². Each surface condition was examined a minimum of three times per sample. The approximate locations of each polarization

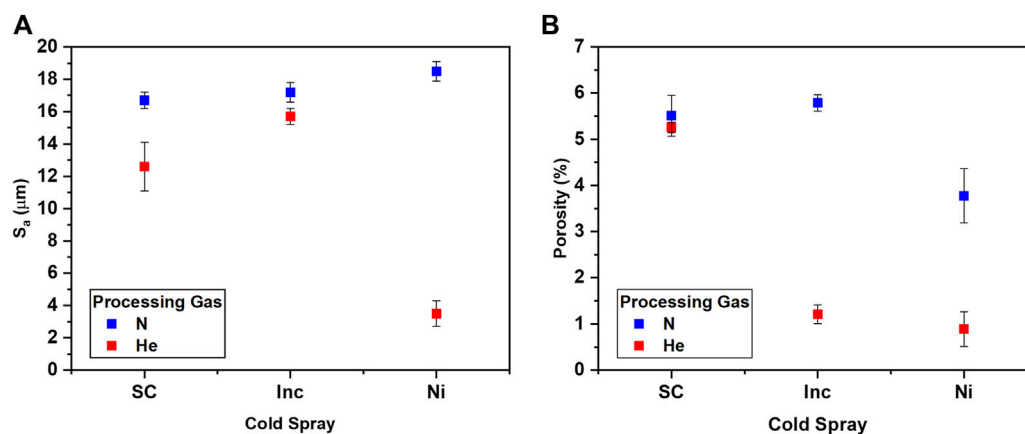
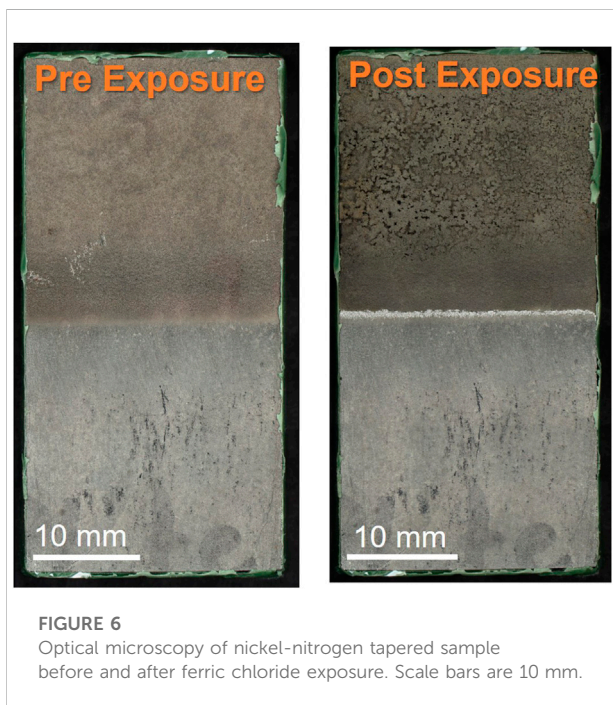
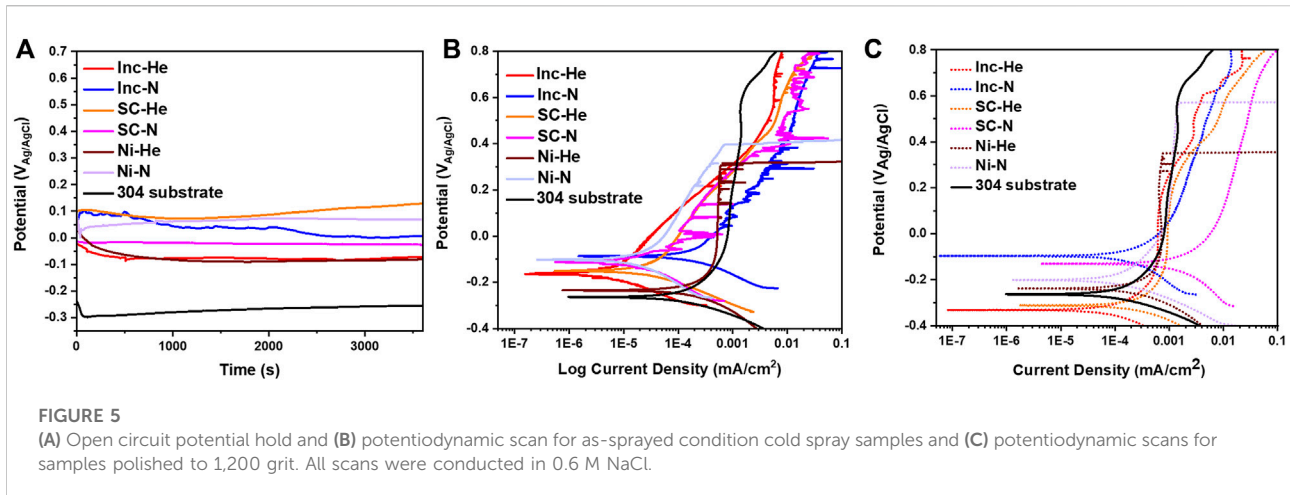


FIGURE 4
(A) Surface roughness and (B) porosity values for cold spray samples.



scan on the cold spray are shown in Figure 2. This o-ring was then epoxied onto a flat cell and secured with a clamp. The flat cell was filled with ~200 ml of aqueous 0.6 M NaCl solution. A counter electrode of platinum mesh and an Ag/AgCl reference electrode were used. On a Biologic SP-300 potentiostat, the samples underwent a potentiodynamic scan from -0.2 vs. OCP to 0.8 V vs. Ag/AgCl at 0.167 mV/s following an hour hold at open circuit potential (OCP). A cut-off current of 100 μ A was employed during the potentiodynamic scan. Post-test the exposed area was measured optically on a Keyence VHX-7000 Digital Microscope and the current density normalized by this area.

Ferric chloride immersion testing

Full immersion pitting tests were performed in accordance with ASTM G48 method A (ASTM, 2015). The sides and bottom of the cold spray samples were coated in epoxy, seen in Figure 3, and optically imaged pre-exposure on a Keyence VHX-7000. Samples were submerged in 6% by mass ferric chloride solution at 22°C for 72 h. At the conclusion of the test, samples were rinsed with deionized water and dried with nitrogen gas. Samples were again optically imaged on a Keyence VHX-7000. Images of the exposed surface were taken on a Zeiss Gemini 500 Field Emission Scanning Electron Microscope. The samples were then cross-sectioned and polished to a mirror finish and imaged with a Keyence VHX-7000. Electron backscatter diffraction (EBSD) was performed on a selection of the cross-sections on a Zeiss Gemini Supra VP55. Diffraction patterns in the cold spray were unobtainable at the resolution used due to the substantial deformation of the cold spray particles. As a result, EBSD focuses on the substrate immediately under the patch edge as well as a region under the full coating thickness, far from the edge and therefore far from any potential corrosion damage.

Results

Surface roughness values, graphed in Figure 4A, were similar, and in general much higher, for all of the nitrogen processed samples. The helium produced much smoother surfaces, particularly in the case of the nickel.

The processing gas selection also influenced the porosity. Helium has been reported to affect the porosity of cold spray coatings (MacDonald et al., 2018). For the materials in this work, the porosity was generally lowered by the use of helium, as seen in Figure 4B. Differences in porosity for Super C are less substantial, but Inconel and nickel show drastic reductions in porosity for the

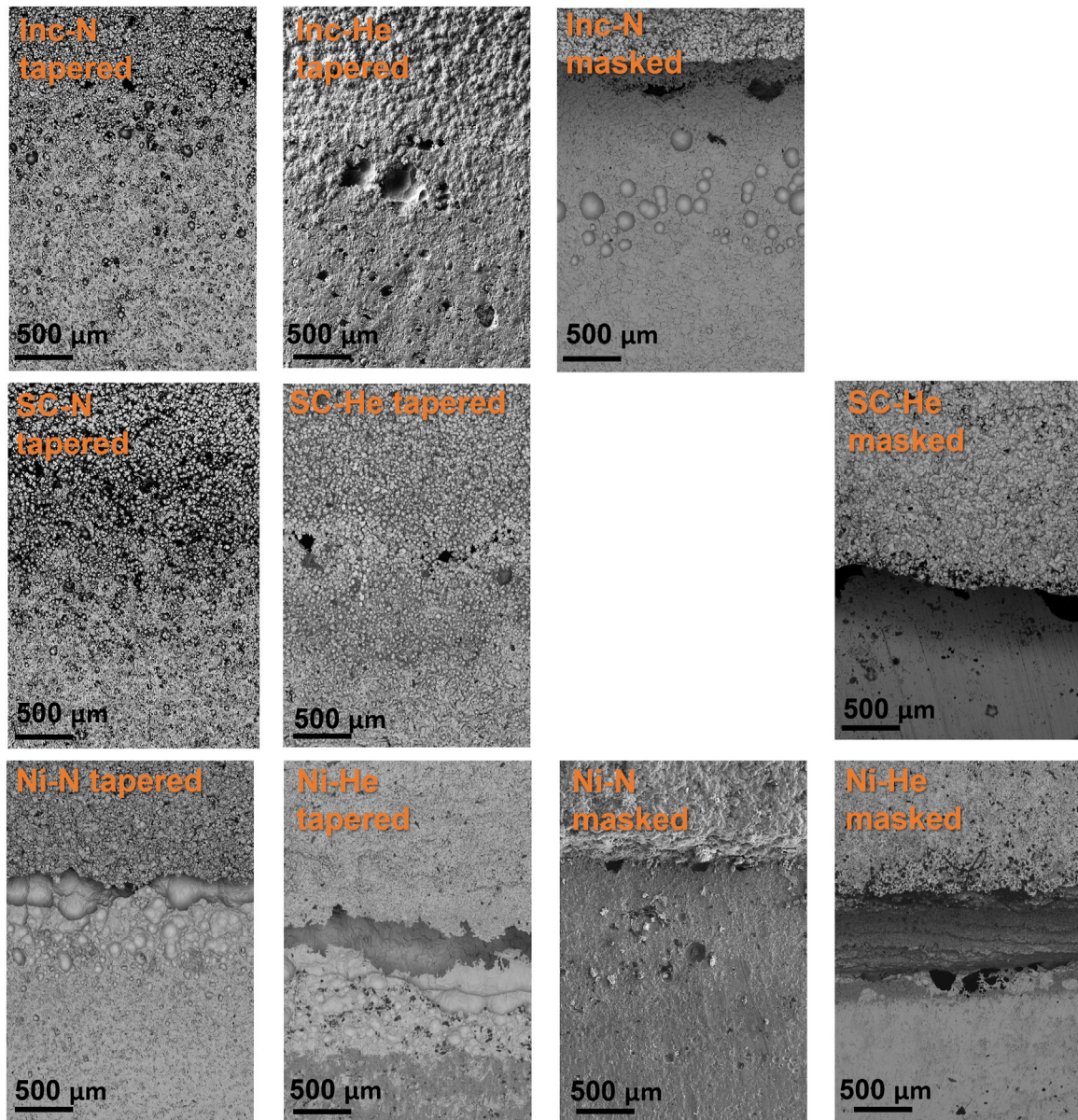


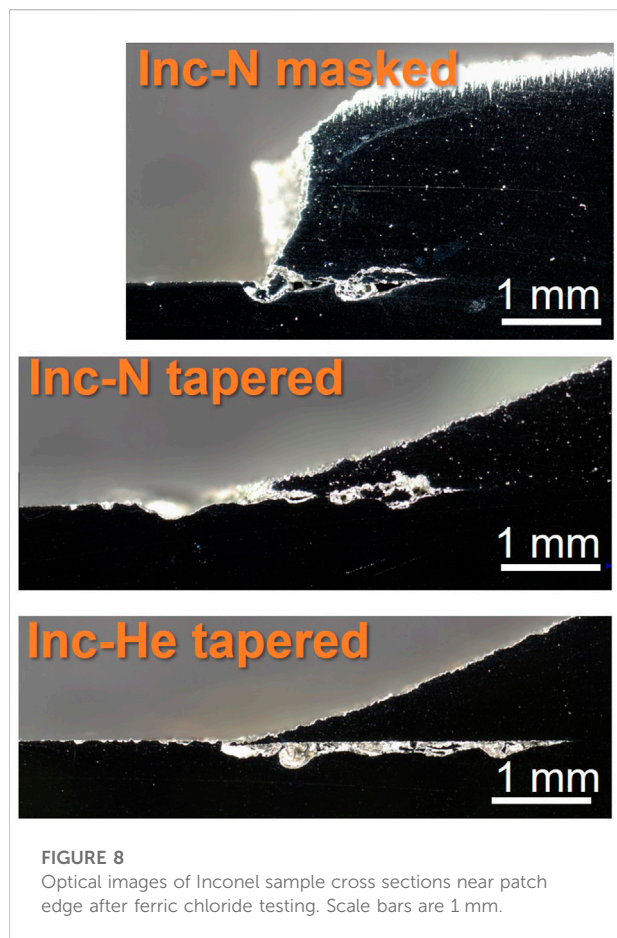
FIGURE 7
SEM of cold spray samples interface region post ferric chloride exposure. Images are oriented with cold spray at the top, substrate on the bottom. Scale bars are 500 μm.

helium processed condition compared to the nitrogen processed conditions. This may be due to the increased kinetic energy of particles as helium has a higher critical velocity compared to nitrogen, potentially leading to increased particle deformation and reduced porosity.

Representative open circuit potentials and electrochemical scans from samples in the as-sprayed condition are presented in [Figure 5A](#) & [Figure 5B](#). A representative scan from the wrought 304 L substrate is also included for comparison. Given the similarities in surface roughness, the current density has not

been corrected for surface roughness. The materials all exhibit metastable pitting, brief increases in current density. Notably the nickel undergoes breakdown at a low potential (between 0.2 and 0.6 V vs. Ag/AgCl). The scan did not continue to high enough voltages to see the breakdown potentials of the other samples.

Comparing the curves for cold spray processed with helium and nitrogen, there are a couple of distinct differences. Inconel and Super C samples processed with helium show less metastable pitting than the nitrogen processed condition. The Inconel and Super C samples also show lower passive current densities for the



helium processed condition. The nickel samples do not exhibit the same trends.

Figure 5C shows electrochemical scans for each sample type in the polished condition. Polishing reduced instances of metastable pitting for all sample types. The early breakdown of the nickel samples persists for the polished conditions. The change in OCP for all samples related to polishing is expected due to mechanical removal of the native oxide.

Post-exposure corrosion damage from the ferric chloride test is readily seen in top-down optical images of the nickel cold spray samples, Figure 6, but is difficult to discern for the Super C and Inconel tapered edge samples. The nickel samples processed with nitrogen for both edge conditions show substantial damage in the cold spray region. Similar damage is not observed in the helium processed samples. However, for all nickel cold spray samples, regardless of processing gas or edge type, significant damage can be seen at the junction between the cold spray and substrate. Higher magnification SEM images in Figure 7 show that the tapered nickel samples, both nitrogen and helium processed, sustained more pitting at the interface than any other sample and this pitting appears to extend underneath the cold spray layer.

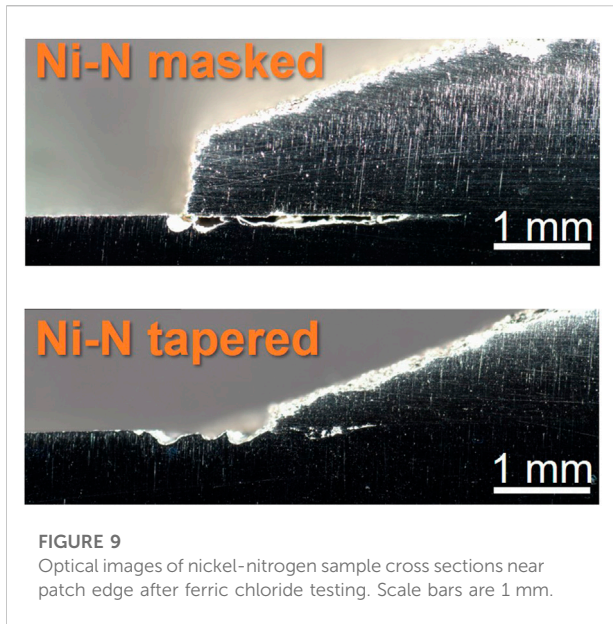
Masked samples of all types showed evidence of corrosion attack along the interface with some large pits; these pits are often stood off from the crevice mouth by a noticeable distance (400 μm –2 mm).

The Super C and Inconel tapered samples display evidence of crevice formation, but the surface roughness associated with the more diffuse edge makes it difficult to get a true sense of the attack in the region from top-down imaging. For Super C and Inconel samples, any damage in the cold spray region was also obscured by the roughness of the coating.

When viewed in cross-section, corrosion damage becomes apparent, as seen in Figure 7. The width and length of the damage that forms underneath the cold spray varies from sample to sample. The cross sections represent only one location in the sample and therefore cannot convey a comprehensive story, but some important information can be obtained. For all samples a noticeable amount of damage can be seen between the cold spray and substrate layers. While this is exacerbated by the aggressive ferric chloride, the damage observed indicates locations where enhanced corrosion may occur in sea salt dominated environments on a cold spray patch. Notably the Inconel processed with nitrogen and the Super C processed with nitrogen appear to have sustained damage both within the cold spray and the substrate along the cross-sectioned interface. The Inconel processed with helium and nickel processed with nitrogen, on the other hand, seem to have contained the corrosion damage to the substrate layer.

EBS and phase contrast images were taken on the cross-section of the cold spray samples were taken at the patch edge and far from the edge (away from the corroded region). The Inconel-nitrogen masked sample is shown in Figure 8 and Figure 9. Deformation appears beneath the cold spray and is contained to the top $\sim 20 \mu\text{m}$ of the substrate material. Additionally, because the substrate material is 304 L stainless steel, the phases detected in the EBS are examined for evidence of increased deformation-induced martensite, which is body-centered cubic (BCC), at the interface. At the scale and resolution examined, no increased presence of BCC phase was found at the surface of the substrate beneath the cold spray seen in Figure 10. No notable differences in BCC phase concentration or deformation layer thickness were found for the other samples examined.

The corrosion damage at the patch edge, seen in Figure 11 for the Inconel-nitrogen masked sample, extends well below the layer of deformation visible in the EBS far from the patch edge. This trend was observed across all the samples examined. Additionally, for all samples this attack narrows as it penetrates further underneath the cold spray (to the right of the patch edge) and may indicate that the progression of corrosion attack is associated initially with this deformation layer.



Discussion

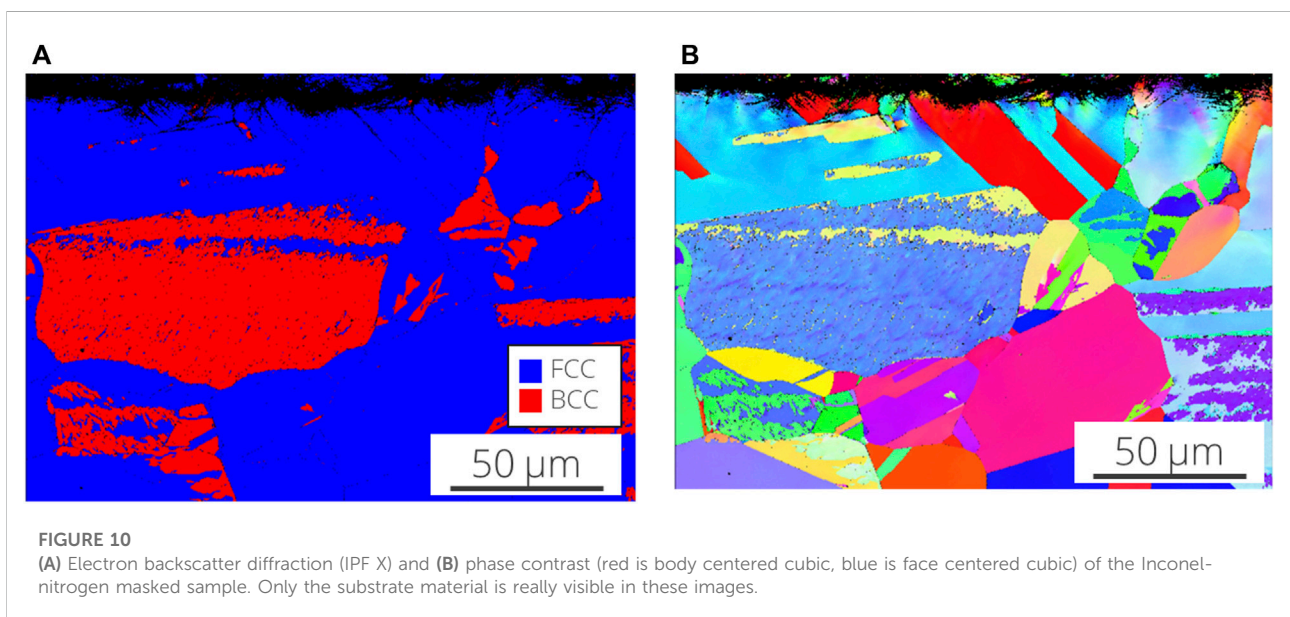
In this study, the corrosion behavior of three different cold spray coatings on wrought 304 L stainless steel was examined. Samples showed variations in corrosion behavior influenced by several variables. These variations being made apparent by the test methodology lends credence to the ability to rapidly down select materials for the purposes of corrosion protection with an emphasis on a patch application scenario. These tests also allowed insight into the factors influencing corrosion behavior of cold sprayed coatings. The nature of the corrosion damage also highlights the need for techniques that can evaluate the

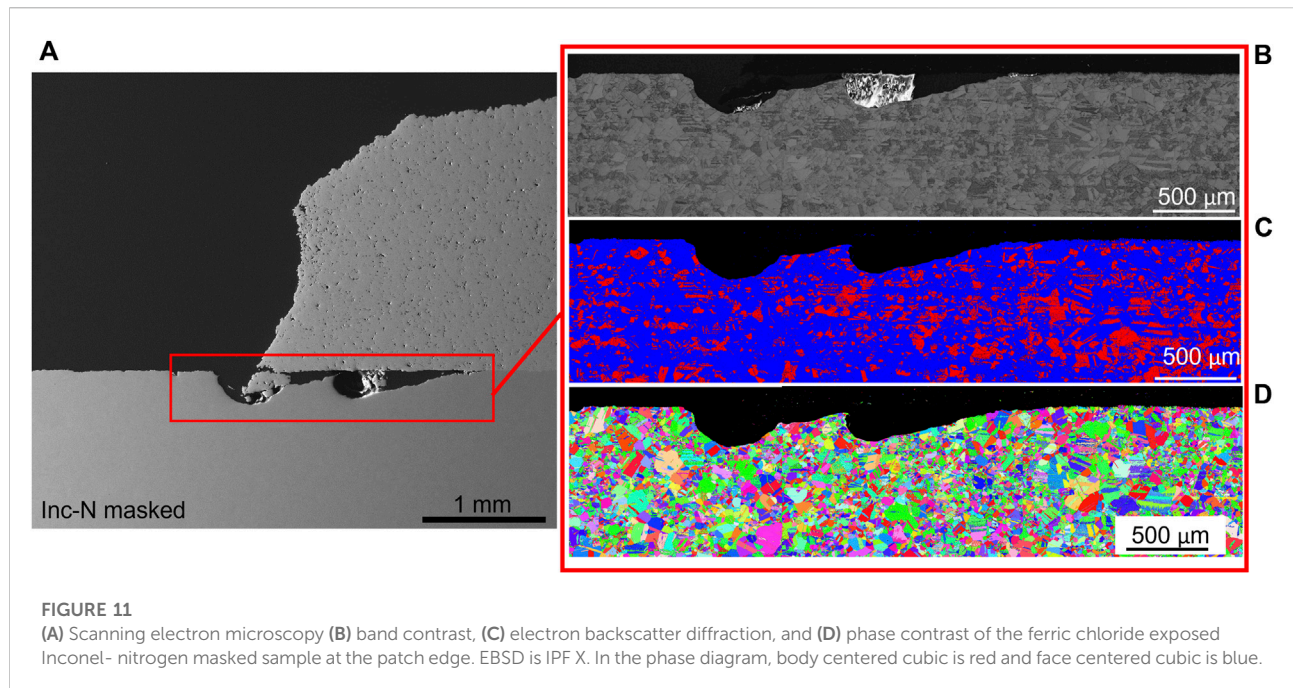
effectiveness of the coating in the field after deployment (Ross et al., 2021; Xia et al., 2022).

The most intuitive variable to influence corrosion behavior is material selection. The impact on the behavior can be seen in the electrochemical scans of the material as well as the ferric chloride exposures. The electrochemical scans indicated, through the lower breakdown potential, that overall the nickel cold spray coatings were likely to have the lowest resistance to pitting. This held true for the ferric chloride exposures with the nickel samples exhibiting the most damage within the cold spray for any of the samples and having extensive pitting damage right at the juncture between cold spray and substrate.

Increased surface roughness and porosity decrease corrosion resistance

The surface roughness contributed to the metastable pitting observed in the polarization scans in Figure 5B. That is, for the polished condition shown in Figure 5C much less metastable pitting is observed. Tortuous surfaces such as those that result from cold spray and AM are known to create occluded sites that increase corrosion susceptibility (Otero et al., 1998; Schaller et al., 2018). Similarly, pores can serve as preferential sites for corrosion (Rosenfeld and Marshakov, 1964; Betts and Boulton, 2013). This has been observed particularly for AM metals where porosity is a common processing defect. In cold spray, as pores form in intersplat regions where full density was not achieved, they are often irregular in shape with sharp features, and are much more analogous to their AM counterparts of lack of fusion pores rather than gas porosity. These sharp featured pores are likely what give rise to the enhanced pitting attack in the as-sprayed cold spray materials (Schaller et al., 2017). The passive current





densities in the polished polarization scans, [Figure 5C](#), evidence the impact of the porosity. For the nickel and Inconel samples, the helium produces more dense coatings ([Figure 4B](#)). The helium processed nickel and Inconel exhibit lower passive current densities than their nitrogen processed counter parts. Interestingly, the Super C samples do not strictly follow this same trend. Helium processed Super C did not produce a substantially lower porosity sample, instead the nitrogen and helium processed samples have very similar porosities. This could be due to the molybdenum content in the Super C which increases work hardenability. In the polished case, the helium processed condition still leads to a lower passive current density, but in the as-sprayed condition the two have very similar current densities, with nitrogen exhibiting more metastable pitting. The minimal differences in surface roughness and porosity between the nitrogen and helium processed Super C samples do not account for the differences in metastable pitting, in the as-printed case, nor the difference in passive current density in the polished condition. Similarly, in the as-sprayed condition the nickel samples processed with helium has more instances of metastable pitting compared to the nitrogen processed samples despite the lower porosity and lower surface roughness of the helium processed condition. These differences in corrosion behavior may be caused by variables such as microstructure or oxides formed during the spraying process. A study focused on the impacts of the spray parameters on these variables would lend more insight but was beyond the scope of this research.

Effects from the porosity are also visible in the ferric chloride testing. The porosity of the cold spray coating impacts the

location of the damage in cross-section, seen in [Figure 8](#) and [Figure 9](#). More porous coatings, >5% porosity such as the Super C-nitrogen and Inconel-nitrogen samples, experienced corrosion attack extending into both the cold spray and the substrate materials along the entire length of the damage. For the coatings with lower porosity, below ~ 4% such as the Inconel-helium sample, the corrosion damage appears to be primarily restricted to the substrate material. This is likely a meaningful trend, but caution should be exercised; these cross-sections only represent attack along one intersection across the cold spray, substrate interface.

Cold spray materials selection influences corrosion and subsequent interface attack

The Inconel and Super C alloys were chosen for their traditionally low galvanic corrosion risk when paired with 304 stainless steels, but this galvanic couple has not been examined for cold sprayed materials. The commercially pure nickel spray, chosen for comparison purposes, did behave more poorly in the ferric chloride when examining the cold spray region. Additionally, the nickel samples sustained a lot more pitting at the edge of the cold spray patch and in the substrate near the edge of the patch, observed in [Figure 12](#) and [Figure 7](#). The Inconel and Super C samples did not experience as severe of attack in the cold spray region as the nickel. In fact, none was visible in the optical images in [Figure 12](#) and even in the [Figure 7](#) SEM images, corrosion damage was not readily apparent in the

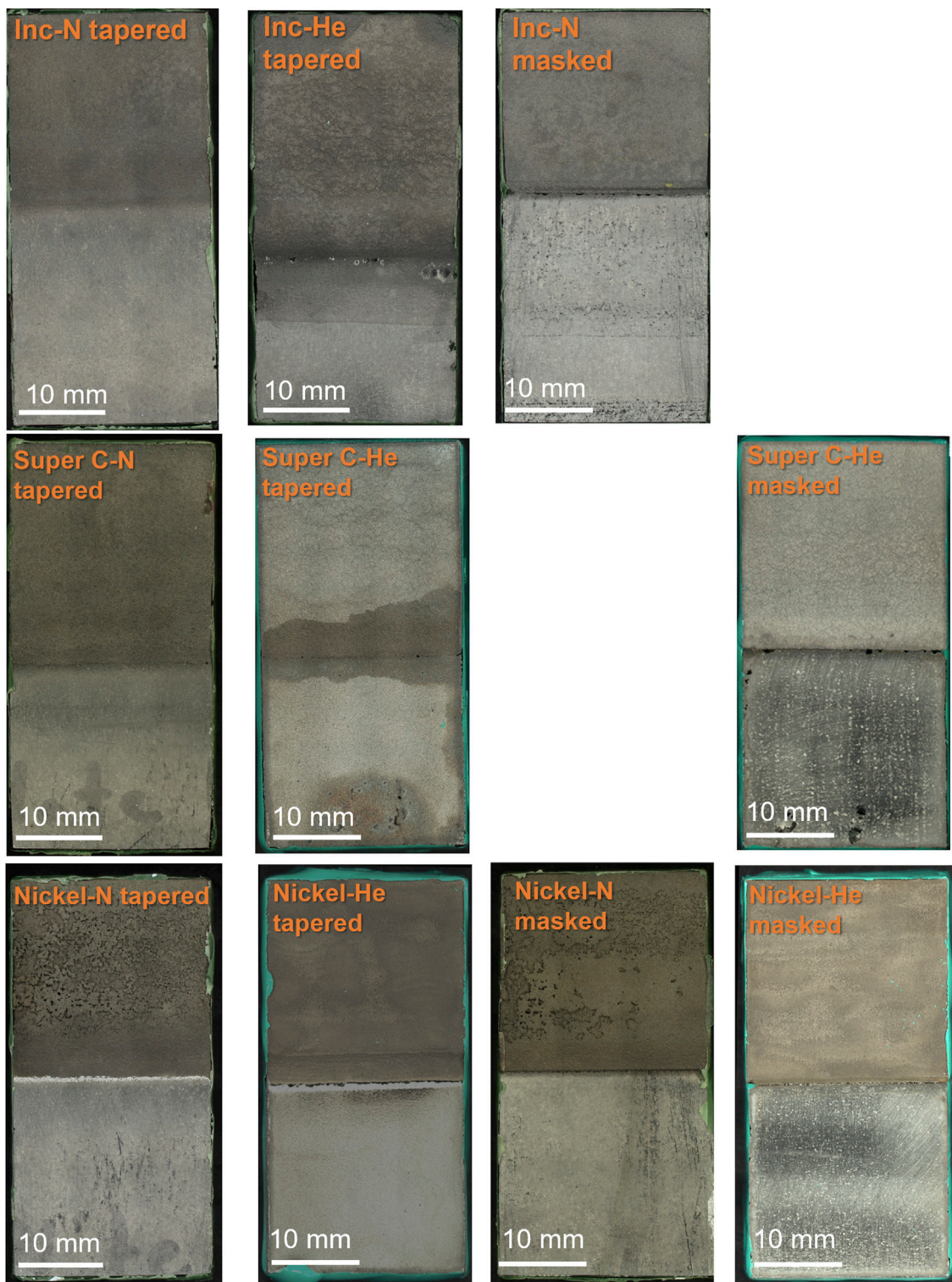


FIGURE 12
Optical microscopy of post ferric chloride exposure cold spray samples. Images are oriented such that the cold spray is on the top half of the image and the 304 L substrate is on the lower half. Scale bars are 10 mm.

cold spray region of the Inconel or Super C. The SEM images at the interface reveal that the damage occurring at the juncture between cold spray and substrate for the Inconel and Super C samples is less severe than those of nickel samples.

Edge type influences corrosion attack

The edge type of the samples changed the appearance of the corrosion attack. Masked samples, in the top-down view, show wider mouth crevices at the interface compared to the tapered samples. For the Inconel and Super C tapered samples, the corrosion morphology is not as readily apparent, instead forming small pits amongst the diffuse cold spray edge and thin, dark regions indicating crevices are seen in the SEM in [Figure 7](#). The nickel tapered samples experienced large amounts of overlapping pitting, while crevice formation predominates in the top-down view of the masked samples.

Discrete cold spray particles on the substrate, such as those that are present in the diffuse edge of the tapered sample, would provide sites vulnerable to local galvanic attack. The geometry of the patch edge could also change the throwing power of the galvanic couple. Modeling results from Turner and Gutierrez showed that a coplanar galvanic couple resulted in a lower corrosion rates than a step-like geometry similar to the masked edge geometry in this study ([Turner and Gutierrez-Miravete, 2013](#)). Using finite element modeling, Marshall et al. reported that a stainless steel and aluminum alloy galvanic couple in immersion conditions could exert substantial galvanic effects up to two inches from the interface between metals ([Marshall et al., 2020](#)). This provides one explanation for how pits formed up to several millimeters from the patch edge in the case of the masked samples.

Deformation layer potentially leads to enhanced corrosion at edges

Despite the substantial corrosion observed in the nickel samples compared to the other samples in [Figure 12](#), particularly in the cold spray region, the corrosion damage is not significantly more severe in cross-section, [Figure 9](#). Galvanic coupling does not explain the extent of the corrosion between the layers, especially in the highly aggressive ferric chloride solution. The EBSD results in [Figure 10](#) and [Figure 11](#) indicate a thin layer of deformation, $\sim 20\ \mu\text{m}$, in the substrate underneath the cold spray coating, likely due to the large kinetic force with which the metal particles impact the substrate. No substantial differences in this deformation layer were observed between sample types, therefore it cannot be the factor influencing the variations in corrosion attack observed in cross section. This deformation could, however, be contributing to the propagation of corrosion between the cold spray and substrate materials which was

observed for all samples tested. 304 stainless steel with a higher dislocation content, like that from deformation, will corrode more easily ([Deng et al., 2017](#); [Wang et al., 2017](#)). No concentration of martensite is seen in the substrate near the interface with the cold spray although diffraction patterns were not able to be obtained from the top $\sim 5\ \mu\text{m}$ of the substrate due to the extent of the deformation. The corrosion is not confined to the deformation layer; the corrosion damage extends beyond the deformation layer visible in the EBSD. The thinner front of corrosion damage underneath the cold spray indicates that the horizontal penetration of the corrosion may, however, be aided by the presence of the deformation. The higher likelihood of metastable pitting for the tortuous as-sprayed surface observed in the electrochemical scans, suggests that it may also be contributing to the development of the interfacial attack. Removing the surface roughness at that interface, particularly in the case of the tapered edge sample, could reduce the likelihood of initiating corrosion between the cold spray and substrate materials.

Conclusion

The work presented in this manuscript aims to help begin filling in a gap in the published literature- the corrosion behavior of metal cold spray coatings. Accelerated corrosion testing, both an electrochemical test and a ferric chloride pitting test, was employed to examine the materials degradation behavior of cold sprayed nickel and nickel-based alloys both separate and in conjunction with a substrate material of 304 L wrought stainless steel. The electrochemical behavior of the cold spray material in 0.6 M NaCl was examined in as-sprayed and ground conditions and compared to the behavior of the substrate. A ferric chloride pitting test was utilized to explore pitting susceptibility at the cold spray edge. The following conclusions can be drawn from these accelerated corrosion tests:

- Helium processing gas reduces porosity and surface roughness as compared to nitrogen.
- Reducing surface roughness through polishing decreases occurrences of metastable pitting in the electrochemical testing.
- Whether damage between the cold spray patch and substrate will extend into the cold spray layer or remain within the substrate is heavily influenced by the porosity of the cold spray.
- Choosing materials historically considered a low galvanic corrosion risk when paired with stainless steels did not eliminate corrosion in the ferric chloride pitting test.
- Although electrochemical characterization of the cold spray coating can provide some indication of the galvanic coupling behavior, it does not fully represent the behavior that will occur at the susceptible patch edge.

- The interface type can influence where the damage occurs (right at or further from the interface).
- Deformation occurring in the substrate beneath the cold spray coating is contributing too, but not the sole influencing factor of, the corrosion occurring between the cold spray and substrate materials.

Data availability statement

The raw data supporting the conclusions of this article will be made available by the authors, without undue reservation.

Author contributions

EK: experiment, investigation, analysis, writing-original draft. TM: experiment, investigation. JT: experiment. KR: sample fabrication, characterization. RS: writing-review and editing, analysis, supervision.

Funding

Sandia National Laboratories is a multitechnology laboratory managed and operated by National Technology and Engineering Solutions of Sandia, LLC, a wholly owned subsidiary of Honeywell International Inc., for the U.S. Department of Energy's National Nuclear Security Administration under contract DE-NA0003525. This paper describes objective technical results and analysis. This article has been authored by an employee of National Technology and Engineering Solutions of Sandia, LLC under Contract No. DE-NA0003525 with the U.S. Department of Energy (DOE). The employee owns all right, title and interest in and to the article and is solely responsible for its contents. The United States

References

- Al-Mangour, B., Vo, P., Mongrain, R., Irissou, E., and Yue, S. (2014). Effect of heat treatment on the microstructure and mechanical properties of stainless steel 316L coatings produced by cold spray for biomedical applications. *J. Therm. Spray. Tech.* 23 (4), 641–652. doi:10.1007/s11666-013-0053-2
- ASTM (2021). Standard test methods for determining area percentage porosity in thermal sprayed coatings. doi:10.1520/e2109-01r21
- ASTM (2015). Standard test methods for pitting and crevice corrosion resistance of stainless steels and related alloys by use of ferric chloride solution.
- Bala, N., Singh, H., Karthikeyan, J., and Prakash, S. (2013). Cold spray coating process for corrosion protection: A review. *Surf. Eng.* 30 (6), 414–421. doi:10.1179/1743294413y.0000000148
- Betts, A. J., and Boulton, L. H. (2013). Crevice corrosion: Review of mechanisms, modelling, and mitigation. *Br. Corros. J.* 28 (4), 279–296. doi:10.1179/000705993799156299
- Champagne, V., and Helfritsch, D. (2014). Critical assessment 11: Structural repairs by cold spray. *Mater. Sci. Technol.* 31 (6), 627–634. doi:10.1179/1743284714y.0000000723
- Champagne, V. K., Champagne, V. K., and Widener, C. (2018). "Cold spray applications," in *Cold-spray coatings* (Berlin, Germany: Springer), 25–56.
- Champagne, V. K., and Helfritsch, D. J. (2014). Mainstreaming cold spray – push for applications. *Surf. Eng.* 30 (6), 396–403. doi:10.1179/1743294414y.0000000277
- Champagne, V. K. (2008). The repair of magnesium rotorcraft components by cold spray. *J. Fail. Anal. Preven.* 8 (2), 164–175. doi:10.1007/s11668-008-9116-y
- Deng, P., Peng, Q., Han, E.-H., and Ke, W. (2017). Effect of the amount of cold work on corrosion of type 304 nuclear grade stainless steel in high-temperature water. *Corrosion* 73 (10), 1237–1249. doi:10.5006/2436
- Dosta, S., Cinca, N., Vilardell, A. M., Cano, I. G., and Guilemany, J. M. (2018). *Cold spray coatings for biomedical applications*. Cold-spray coatings. Cham: Springer, 533–557.
- Eiselstein, H. L., and Tillack, D. J. (1991). The invention and definition of alloy 625. *Superalloys* 718.
- Hassani-Gangaraj, S. M., Moridi, A., and Guagliano, M. (2015). Critical review of corrosion protection by cold spray coatings. *Surf. Eng.* 31 (11), 803–815. doi:10.1179/1743294415y.0000000018

Government retains and the publisher, by accepting the article for publication, acknowledges that the United States Government retains a non-exclusive, paid-up, irrevocable, world-wide license to publish or reproduce the published form of this article or allow others to do so, for United States Government purposes. The DOE will provide public access to these results of federally sponsored research in accordance with the DOE Public Access Plan <https://www.energy.gov/downloads/doe-public-access-plan>. This document is SAND2022-15605 J.

Acknowledgments

The authors wish to thank John Williard and Sara Dickens at Sandia for SEM and EBSD collection and Mayur Pole at Pacific Northwest for porosity and roughness measurements. Special thanks to Charles Bryan, Ryan Katona, Mike Kracum, Brendan Nation, and Andrew Knight at Sandia for their discussions on this research.

Conflict of interest

The authors declare that the research was conducted in the absence of any commercial or financial relationships that could be construed as a potential conflict of interest.

Publisher's note

All claims expressed in this article are solely those of the authors and do not necessarily represent those of their affiliated organizations, or those of the publisher, the editors and the reviewers. Any product that may be evaluated in this article, or claim that may be made by its manufacturer, is not guaranteed or endorsed by the publisher.

- Huang, P., Liu, R., Wu, X. J., and Yao, M. X. (2007). Mechanical properties and corrosion resistance of a novel Ni-Cr-Mo alloy. *Adv. Eng. Mat.* 9 (1-2), 60-64. doi:10.1002/adem.200600160
- Jiang, X., Overman, N., Smith, C., and Ross, K. (2020). Microstructure, hardness and cavitation erosion resistance of different cold spray coatings on stainless steel 316 for hydropower applications. *Mater. Today Commun.* 25, 101305. doi:10.1016/j.mtcomm.2020.101305
- Karasz, E., Taylor, J., Autenrieth, D., Reu, P., Johnson, K., Melia, M., et al. (2021). Measuring the residual stress and stress-corrosion cracking susceptibility of additively manufactured 316l by astm G36-94. *Corrosion* 78, 3. doi:10.5006/3894
- Karthikeyan, J. (2005). Cold spray technology. *Adv. Mater. Process.* 163 (3), 33-35.
- Kumar, S., Kumar, M., and Jindal, N. (2020). Overview of cold spray coatings applications and comparisons: A critical review. *World J. Eng.* 17 (1), 27-51. doi:10.1108/wje-01-2019-0021
- Lee, J. H., Jang, H. L., Lee, K. M., Baek, H. R., Jin, K., Hong, K. S., et al. (2013). *In vitro* and *in vivo* evaluation of the bioactivity of hydroxyapatite-coated polyetheretherketone biocomposites created by cold spray technology. *Acta Biomater.* 9 (4), 6177-6187. doi:10.1016/j.actbio.2012.11.030
- Leyman, P. F., and Champagne, V. K. (2009). Cold spray process development for the reclamation of the Apache helicopter mast support. Contract No.: ARL-TR-4922.
- Luzin, V., Kuroda, S., Yin, S., and Ang, A. S. M. (2020). Advanced residual stress analysis in thermal spray and cold spray processes. *J. Therm. Spray Technol.* 29 (6), 1211-1217. doi:10.1007/s11666-020-01083-w
- MacDonald, D., Rahmati, S., Jodoin, B., and Birtch, W. (2018). An economical approach to cold spray using in-line nitrogen-helium blending. *J. Therm. Spray. Tech.* 28 (1-2), 161-173. doi:10.1007/s11666-018-0813-0
- Marshall, R. S., Goff, A., Sprinkle, C., Britos, A., and Kelly, R. G. (2020). Estimating the throwing power of Ss316 when coupled with Aa7075 through finite element modeling. *Corrosion* 76, 476-484. doi:10.5006/3438
- Nardi, A. (2019). *Cold spray coatings for Cr and Ni plating replacement*. Maryland, United States: US Army Research Laboratory.
- Otero, E., Pardo, A., Utrilla, M. V., Sáenz, E., and Álvarez, J. F. (1998). Corrosion behaviour of aisi 304l and 316l stainless steels prepared by powder metallurgy in the presence of sulphuric and phosphoric acid. *Corros. Sci.* 40, 1421-1434. doi:10.1016/s0010-938x(98)00047-x
- Papyrin, A. (2001). *Cold spray Technology*. Amsterdam, Netherlands: Elsevier, 336. Advanced Materials & processes.
- Qu, H. J., Srinivasan, J., Zhao, Y., Mao, K. S., Taylor, J. M., Marino, G., et al. (2022). Stress corrosion cracking mechanism of cold spray coating on a galvanically similar substrate. *Mater. Sci. Eng. A* 849, 143404. doi:10.1016/j.msea.2022.143404
- Rokni, M. R., Nutt, S. R., Widener, C. A., Champagne, V. K., and Hrabe, R. H. (2017). Review of relationship between particle deformation, coating microstructure, and properties in high-pressure cold spray. *J. Therm. Spray. Tech.* 26 (6), 1308-1355. doi:10.1007/s11666-017-0575-0
- Rosenfeld, I. L., and Marshakov, I. K. (1964). Mechanism of crevice corrosion. *Corrosion* 20, 115-125. doi:10.5006/0010-9312-20.4.115t
- Ross, K. A., Lareau, J. P., Glass, S. W., and Meyer, R. M. (2021). *Assessment of cold spray Technology for nuclear power applications*. United States: Pacific Northwest National Laboratory. Contract No.: PNNL-30299.
- Sample, C. M., Champagne, V. K., Nardi, A. T., and Lados, D. A. (2020). Factors governing static properties and fatigue, fatigue crack growth, and fracture mechanisms in cold spray alloys and coatings/repairs: A review. *Addit. Manuf.* 36, 101371. doi:10.1016/j.addma.2020.101371
- Schaller, R. F., Mishra, A., Rodelas, J. M., Taylor, J. M., and Schindelholz, E. J. (2018). The role of microstructure and surface finish on the corrosion of selective laser melted 304l. *J. Electrochem. Soc.* 165 (5), C234-C242. doi:10.1149/2.0431805jes
- Schaller, R. F., Taylor, J. M., Rodelas, J., and Schindelholz, E. J. (2017). Corrosion properties of powder bed fusion additively manufactured 17-4 Ph stainless steel. *Corrosion* 73 (7), 796-807. doi:10.5006/2365
- Schneider, C. A., Rasband, W. S., and Eliceiri, K. W. (2012). Nih image to imagej: 25 Years of image analysis. *Nat. Methods* 9 (7), 671-675. Epub 2012/08/30. doi:10.1038/nmeth.2089
- Ševeček, M., Gurgun, A., Seshadri, A., Che, Y., Wagih, M., Phillips, B., et al. (2018). Development of Cr cold spray-coated fuel cladding with enhanced accident tolerance. *Nucl. Eng. Technol.* 50 (2), 229-236. doi:10.1016/j.net.2017.12.011
- Singh, H., Sidhu, T. S., and Kalsi, S. B. S. (2012). Cold spray technology: Future of coating deposition processes. *Frat. Ed. Integrità Strutt.* 6 (22), 69-84. doi:10.3221/igf-esis.22.08
- Singh, R., Bashir, H., and Kumar, R. (2021). Hybrid heat sink manufacturing by cold spray: Hybrid heat sinks produced via cold spray technology can be a cost effective and lightweight Alternative for cooling electronics. *Semin. Cancer Biol.* 179 (3), 37-52. doi:10.1016/j.semcancer.2020.06.008
- Smith, M. F. (2016). "Introduction to cold spray," in *High pressure cold spray-principles and applications*. Editors C. M. Kay and J. Karthikeyan (Ohio: ASM International).
- Soboň, D. (2018). "Application of cold sprayed coatings in aviation and automotive," in XI International Science-Technical Conference Automotive Safety, Slovakia, 18-20 April 2018 (IEEE).
- Sohag, F. A., Beck, F. R., Mohanta, L., Cheung, F.-B., Segall, A. E., Eden, T. J., et al. (2017). Enhancement of downward-facing saturated boiling heat transfer by the cold spray technique. *Nucl. Eng. Technol.* 49 (1), 113-122. doi:10.1016/j.net.2016.08.005
- Sova, A., Grigoriev, S., Okunkova, A., and Smurov, I. (2013). Potential of cold gas dynamic spray as additive manufacturing technology. *Int. J. Adv. Manuf. Technol.* 69 (9-12), 2269-2278. doi:10.1007/s00170-013-5166-8
- Teague, M., Saltzstein, S., Hanson, B., Sorenson, K., and Freeze, G. (2019). Gap analysis to guide doe R&D in supporting extended storage and transportation of spent nuclear fuel: An FY2019 assessment. Contract No.: SAND2019-15479R.
- ToolBox (2009). Metals in seawater - galvanic series. [cited 2022]. Available from: https://www.engineeringtoolbox.com/metals-galvanic-series-seawater-d_1495.html.
- Toribio, J. (1998). Residual stress effects in stress-corrosion cracking. *J. Mater. Eng. Perform.* 7, 173-182. doi:10.1361/105994998770347891
- Turner, M., and Gutierrez-Miravete, E. (2013). "Modeling galvanic corrosion," in COMSOL Conference, Boston.
- Umretiya, R. V., Elward, B., Lee, D., Anderson, M., Rebak, R. B., and Rojas, J. V. (2020). Mechanical and chemical properties of pvd and cold spray Cr-coatings on zircaloy-4. *J. Nucl. Mater.* 541, 152420. doi:10.1016/j.jnucmat.2020.152420
- Vilardell, A. M., Cinca, N., Concustell, A., Dosta, S., Cano, I. G., and Guilemany, J. M. (2015). Cold spray as an emerging technology for biocompatible and antibacterial coatings: State of art. *J. Mat. Sci.* 50 (13), 4441-4462. doi:10.1007/s10853-015-9013-1
- Wang, J., Lu, H., Zhang, L., Meng, F., and Xu, X. (2017). Effects of dissolved gas and cold work on the electrochemical behaviors of 304 stainless steel in simulated pwr primary water. *Corrosion* 73 (3), 281-289. doi:10.5006/2221
- Widener, C. A., Carter, M. J., Ozdemir, O. C., Hrabe, R. H., Hoiland, B., Stamey, T. E., et al. (2015). Application of high-pressure cold spray for an internal bore repair of a navy valve actuator. *J. Therm. Spray. Tech.* 25 (1-2), 193-201. doi:10.1007/s11666-015-0366-4
- Widener, C. A., Ozdemir, O. C., and Carter, M. (2018). Structural repair using cold spray technology for enhanced sustainability of high value assets. *Procedia Manuf.* 21, 361-368. doi:10.1016/j.promfg.2018.02.132
- Xia, D.-H., Deng, C.-M., Macdonald, D., Jamali, S., Mills, D., Luo, J.-L., et al. (2022). Electrochemical measurements used for assessment of corrosion and protection of metallic materials in the field: A critical review. *J. Mater. Sci. Technol.* 112, 151-183. doi:10.1016/j.jmst.2021.11.004
- Yeom, H., Dabney, T., Pocquette, N., Ross, K., Pfeifferkorn, F. E., and Sridharan, K. (2020). Cold spray deposition of 304l stainless steel to mitigate chloride-induced stress corrosion cracking in canisters for used nuclear fuel storage. *J. Nucl. Mater.* 538, 152254. doi:10.1016/j.jnucmat.2020.152254
- Yeom, H., and Sridharan, K. (2021). Cold spray technology in nuclear energy applications: A review of recent advances. *Ann. Nucl. Energy* 150, 107835. doi:10.1016/j.anucene.2020.107835
- Yin, S., Cavaliere, P., Aldwell, B., Jenkins, R., Liao, H., Li, W., et al. (2018). Cold spray additive manufacturing and repair: Fundamentals and applications. *Addit. Manuf.* 21, 628-650. doi:10.1016/j.addma.2018.04.017